Computation and Turbulence Modeling for Three-Dimensional Boundary Layers Including Turbomachinery Rotor Flows

J. Zhang* and B. Lakshminarayana†
Pennsylvania State University, University Park, Pennsylvania

A method is developed for predicting the behavior of three-dimensional, turbulent boundary layers occurring in internal flows, including those on turbomachinery rotor blades. These boundary layers are complex, turbulent, and subject to Coriolis and centrifugal forces. The major thrust of this paper is the development and use of an algebraic Reynolds stress model (ARSM) that captures the changes in turbulent flow structure arising from curvature, rotation, and three dimensionality. The prediction of pressure-driven secondary flow agrees well with the measured data, and all three turbulence models (k-ε, algebraic eddy viscosity, and ARSM) show the same level of agreement. The prediction of boundary-layer development on rotor blades shows much better agreement with measurements with the ARSM. It is essential to employ higher-order turbulence models to capture the effects of rotation, curvature, and three dimensionality on boundary layers in turbomachinery.

Nomenclature

C_s	= constant
c_μ	= turbulent transport coefficient in k-ε model
F	= nondimensional velocity U_1/U_{ref}
G	= nondimensional velocity U_2/U_{ref}
H_i	= matrix scale coefficient in surface coordinates
k	= turbulent kinetic energy
L	= reference length scale
P	= static pressure
P_k	= production of turbulent kinetic energy
Q_e	= total freestream velocity
R	= radius normalized by annulus wall radius
R_e	= Reynolds number
S,N,R	= coordinates in streamwise, normal, and radial directions normalized by local chord length, local chord length, and annulus wall radius, respectively
U_s,V_n,W_r	= relative mean velocity in streamwise, normal, and radial directions, respectively
U_1,U_2,U_3	= velocity components in surface coordinate system (Fig. 1)
U_τ	= wall friction velocity
u_i	= velocity fluctuation
$\overline{u_i u_j}$	= Reynolds stress tensor (τ_{ij})
x_1,x_2,x_3	= surface coordinates (Fig. 1)
y	= distance from the wall or blade surface
y^+	= wall distance variable
δ_{ij}	= Kronecker delta
ε	= turbulent dissipation
ε_{ijk}	= permutation tensor
Θ	= nondimensional temperature T/T_{ref}
μ	= molecular viscosity
μ_t	= eddy viscosity
ξ_1,ξ_2,ξ_3	= independent variables in Levy-Lee transformation
ρ	= density
ϕ	= mass-averaged flow coefficient (normalized by blade-tip speed)
Ω	= angular velocity
Ω_i	= component of angular velocity vector in surface coordinate, $i = 1,2,3$

Subscripts

e	= edge of boundary layers
i,j,k	= denoting coordinate direction
ref	= reference
w	= wall
∞	= far stream

Introduction

THE boundary layers developing on turbomachinery rotor blades are complex, turbulent, three dimensional, and subject to centrifugal and Coriolis forces. Navier-Stokes codes cannot efficiently or accurately resolve these viscous layers because of grid limitations imposed by the size and speed of current computers. The development of prediction techniques that can resolve flows near blade surfaces are necessary for design and analysis of turbomachinery. It is essential to develop an accurate and rapid method of predicting the behavior of the viscous layers on turbomachinery rotor blades. Hence, boundary-layer techniques become very attractive.

Some of the earlier techniques for the prediction of three-dimensional, turbulent boundary-layer development on turbomachinery blades were based on either the momentum integral technique[1] or the quasi-three-dimensional solution.[2] Thompkins and Usab[2] assumed that crossflow was small, thus, uncoupling the two momentum equations.

External aerodynamicists have successfully employed boundary-layer techniques/codes to predict flow over external surfaces such as wings.[3,4] A review of the various boundary-layer techniques in external flow applications is given in Refs. 3, 5, and 6. One successful application of these techniques to a turbomachinery blade is described in Refs. 7-9.

Vatsa[7] and Anderson[8,9] made an attempt to predict general three-dimensional, turbulent boundary-layer development on turbomachinery rotor blades, which includes 1) the construction of a general surface coordinate system for twisted turbine blades; 2) the development of a method to calculate the boundary-layer edge conditions from a known static pressure distribution; 3) the derivation of the three-dimensional

boundary-layer equations in a general rotating coordinate system in which the Coriolis force appears explicitly; and 4) the formulation of a generalized Levy-Lee transformation. Heat transfer and total pressure levels on a turbine blade were computed using this code. However, the calculation used an eddy viscosity turbulence model, which could not account for curvature, rotation, and other complex effects. Furthermore, these authors showed no comparisons with boundary profile data. In this paper, a generalized algebraic Reynolds stress model (ARSM) is developed, and the computational method based on Refs. 7 and 8 is modified to include this model. The turbulent kinetic energy and the dissipation rate are determined from the respective transport equations. Computation of the behavior of a pressure-driven, three-dimensional boundary layer and of the boundary layers on a compressor rotor blade are carried out.

Turbulent flow modeling is an important feature in the computation of three-dimensional boundary layers on turbomachinery blade surfaces. To predict three-dimensional, blade boundary layers accurately, a proper turbulence model should be incorporated into the computation. A comprehensive survey of turbulence models used in engineering applications is given in Ref. 10, which carries out a critical review of zero-equation, one-equation, two-equation, algebraic Reynolds stress and full Reynolds stress models, and recommends that either the full Reynolds stress equations or algebraic Reynolds stress equations should be employed to describe the three-dimensional, boundary-layer properties accurately when rotation and curvature effects are present. A new ARSM model was developed and incorporated into a boundary-layer code. This is the major thrust of the present paper. The model is intended to account for complex turbulence effects in three-dimensional boundary layers. Comprehensive computations were carried out with this model.

Governing Equations

The three-dimensional, boundary-layer equations in terms of a rotating coordinate system (see Fig. 1) are derived in Ref. 7. The equations, after applying the Levy-Lee transformation, are

x_1-Momentum equation

$$\frac{\partial}{\partial \zeta_3}\left(\frac{\bar{\mu}_1}{\bar{\mu}_{\text{ref}}}\frac{\partial F}{\partial \zeta_3}\right) - V\frac{\partial F}{\partial \zeta_3} - C_1 F\frac{\partial F}{\partial \zeta_1} - C_2 G\frac{\partial F}{\partial \zeta_2} - C_{12}F^2 - C_{13}GF$$

$$- C_7 G^2 + C_9 F + C_8 G + C_{14}\Theta + C_{15} = 0 \tag{1}$$

x_2-Momentum equation

$$\frac{\partial}{\partial \zeta_3}\left(\frac{\bar{\mu}_2}{\bar{\mu}_{\text{ref}}}\frac{\partial G}{\partial \zeta_3}\right) - V\frac{\partial G}{\partial \zeta_3} - C_1 F\frac{\partial G}{\partial \zeta_1} - C_2 G\frac{\partial G}{\partial \zeta_2} - C_{27}G^2 - C_{28}FG$$

$$- C_{23}G - C_{20}F^2 - C_{24}F + C_{30}\Theta + C_{29} = 0 \tag{2}$$

Continuity equation

$$\frac{\partial V}{\partial \zeta_3} + C_1\frac{\partial F}{\partial \zeta_1} + C_2\frac{\partial G}{\partial \zeta_2} + C_{45}G + C_{46}F = 0 \tag{3}$$

In Eqs. (1–3), F and G are nondimensionalized velocities (U_1, U_2) in the ζ_1 and ζ_2 directions, respectively and V is the transformed velocity (U_3) derived by integrating the continuity equation. Expressions for coefficients C_1 to C_{46} and V are given in Ref. 8.

The independent variables used in the generalized Levy-Lee transformation are defined by

$$\zeta_1 = \int_0^{x_1} q_0 \, \mathrm{d}x_1 \tag{4}$$
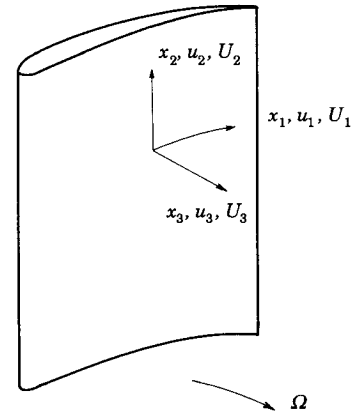

Fig. 1 Coordinate system for three-dimensional boundary-layer computation.

$$\zeta_2 = x_2 \tag{5}$$

$$\zeta_3 = \frac{U_{1e}H_2}{\sqrt{2\zeta_1}}\int_0^{x_3} \rho \, \mathrm{d}x_3 \tag{6}$$

where

$$q = \rho_e U_{1e} H_1 H_2^2 \mu_e \bar{\mu}_{\text{ref}}$$

$$q_0 = q(x_1, 0)$$

$$\bar{\mu}_1 = 1 + \Gamma\frac{\mu_{tl}}{\mu}$$

$$\bar{\mu}_{\text{ref}} = 1 + \Gamma\left(\frac{\mu_{tl}}{\mu}\right)_e$$

and

$$\Gamma = 1 - \exp\left[-4.6513\left(\frac{S - S_{T1}}{S_{T2} - S_{T1}}\right)^2\right]$$

which is the transition model developed in Ref. 11. Here, S_{T1} and S_{T2} are the specified locations for the beginning and the end of transition, respectively.

Algebraic Reynolds Stress Model

It is well known that the eddy viscosity and k-ϵ models do not capture the flow physics associated with three dimensionality, curvature, and rotation.[10] The following conclusions are based upon a recent review[10] of various turbulence models and a comparison with the data available for complex flows.

1) The algebraic eddy viscosity model is valid only for two-dimensional flows with mild pressure gradient and with no rotation or curvature effects.

2) The k-ϵ model is good for most two-dimensional, unseparated flows, but this model cannot capture rotation and curvature effects.

3) In the presence of complex strain effects (rotation, curvature, separation, three dimensionality), the most suitable model is the full Reynolds stress equations. This model can provide a more realistic and rigorous approach to turbulence modeling. However, the Reynolds stress equations are extremely complicated for a three-dimensional flow. There are six Reynolds stress transport equations resulting in 10–12 transport equations for the mean flow and turbulence quantities. This is prohibitive from a computational standpoint. Therefore, much effort has been expended to use simplified Reynolds stress equations.

4) The algebraic Reynolds stress equations provide accurate predictions for most complex engineering flows. These algebraic equations, solved in combination with transport

equations for k and ϵ, provide a true representation of the flow physics. The curvature, rotation, and other complex strain effects in the mean flow appear explicitly in the algebraic Reynolds stress equations.

In simplifying the Reynolds stress equation, the transport terms (diffusion and convection) in the modeled Reynolds stress equation are assumed to be proportional to the transport terms in the turbulent kinetic energy equation. The parameter of proportionality is $\overline{u_i u_j}/k$. Rodi[12] suggested this approach. Galmes and Lakshminarayana[13] further extended it to include the effect of rotation.

Rodi and Scheuerer[14] made a systematic comparison of data and computation for curved shear flow with various turbulence models and observed that the ARSM model (derived from the full Reynolds stress equation in a curvilinear system) captured the physics associated with the effect of curvature on turbulence structure. Likewise, Warfield and Lakshminarayana[15] provided comparisons for a rotating duct and demonstrated that the k-ϵ and the algebraic eddy viscosity models failed to capture the effect of rotation on the boundary layer for a duct rotating about a spanwise axis. The rotation has a destabilizing (amplifying) effect on the leading side of the channel and stabilizing (attenuating) effect on the trailing side. This introduces asymmetry in the velocity profile about the duct centerline. Both the k-ϵ and the algebraic eddy viscosity models, in which the rotation effects do not appear explicitly or implicitly, fail to capture this effect resulting in poor mean velocity and turbulence flow predictions (see Fig. 7 of Ref. 15). The ARSM model, based upon the full Reynolds stress equation in a rotating coordinate system, provides the best predictions. It should be emphasized that the ARSM model, derived in Ref. 12, does not include the curvature or rotation effect.

It is clear that ARSM is the only model which can provide meaningful predictions of internal flows subjected to curvature and rotation. The models used in Refs. 12–15 were based on full Reynolds stress models that neglected the "realizability" condition. Shih and Lumley[16] recently introduced a new model that satisfies invariance and realizability conditions. The invariance condition requires that the modeled terms have the same tensor order as the original terms in order to correctly transform the coordinates. The realizability condition requires that the diagonal terms of the stress tensor remain positive, and the Schwarz inequality hold for all the nondiagonal terms. This model is used in this paper to develop a new algebraic Reynolds stress model. The rotation term is included. The new model is capable of capturing the near-wall physics more accurately, as discussed in Ref. 16.

The Reynolds stress equation modeled by Shih and Lumley,[16] modified to include rotation effects, is given by

$$\frac{D\overline{u_i u_j}}{Dt} = C_s \frac{\partial}{\partial x_k}\left(\frac{k}{\epsilon}\overline{u_k u_l}\frac{\partial \overline{u_i u_j}}{\partial x_l}\right) - \overline{u_i u_k}\frac{\partial U_j}{\partial x_k} - \overline{u_j u_k}\frac{\partial U_i}{\partial x_k}$$

$$+ 2\frac{\partial U_p}{\partial x_q}(I_{pjqi}^{(0)} + I_{piqj}^{(0)}) - \left(\phi_{ij}^{(0)} + \frac{2}{3}\delta_{ij}\right)\epsilon$$

$$+ \left[4C_1 k\left(\frac{\partial U_i}{\partial x_j} + \frac{\partial U_j}{\partial x_i}\right) + C_2 b_{ij}\epsilon\right]$$

$$\times \frac{l}{y}F^\alpha - \Omega_p(\varepsilon_{ipk}\overline{u_j u_k} + \varepsilon_{jpk}\overline{u_i u_k}) \tag{7}$$

where ϵ_{ipk} is the permutation tensor, C_s is a constant, Ω_p is the component of the rotation tensor, and

$$I_{pjqi}^{(0)} = \frac{2k}{30}(4\delta_{pj}\delta_{qi} - \delta_{\delta_{pq}}\delta_{ij} - \delta_{qi}\delta_{pi}) - \frac{2k}{3}(\delta_{qi}b_{pj} - \delta_{pj}b_{qi})$$

$$- \frac{2k}{10}C_{1i}\left(\delta_{pq}b_{ij} + \delta_{ij}b_{pq} + \delta_{qi}b_{pi} + \delta_{pi}b_{qj} - \frac{11}{3}\delta_{qi}b_{pi}\right.$$

$$-\frac{4}{3}\delta_{pj}b_{qi}\right) + \left(\frac{2k}{10}\right)C_{2f}(2\delta_{pj}b_{qi}^2 - 3b_{pq}b_{ij} - 3b_{qj}b_{pi} + b_{qi}b_{pj})$$

$$\phi_{ij}^{(0)} = \beta b_{ij}, \qquad b_{ij} = \frac{\overline{u_i u_j}}{2k} - \frac{1}{3}\delta_{ij}, \qquad b_{qi}^2 = b_{qk}b_{ki}$$

$$\frac{l}{y} = C_3\frac{(2k)^{3/2}}{\epsilon y}, \qquad C_3 = \frac{\epsilon y}{(2k)^{3/2}} \quad \text{when } y \to 0$$

$$C_1 = 0.01, \qquad C_2 = 7.5$$

$$C_{1f} = 1 + 0.8\sqrt{F}, \qquad C_{2f} = 1 - \sqrt{F}$$

$$F = 1 + 27III + 9II, \qquad \alpha = 0.5$$

$$II = -\frac{b_{ij}b_{ji}}{2}, \qquad III = \frac{b_{ij}b_{jk}b_{ki}}{3}$$

$$\beta = 2 + \exp\left(\frac{-7.77}{\sqrt{R_l}}\right)\left\{\frac{72}{\sqrt{R_l}}\right.$$

$$+ 80.1\,\ell n[1 + 62.4(-II + 2.3III)]\left\}\left(\frac{F}{9}\right)\right.$$

$$R_l = \frac{(2k)^2}{9\epsilon v}$$

Using the algebraic transformation,[12] where the ratio of the transport terms in the Reynolds stress equation to the transport terms in the turbulent kinetic energy equation is assumed to be proportional to $\overline{u_i u_j}/k$,

$$\frac{D\overline{u_i u_j}}{Dt} - C_s\frac{\partial}{\partial x_k}\left(\frac{k}{\epsilon}\overline{u_k u_l}\frac{\partial \overline{u_i u_j}}{\partial x_l}\right) = \frac{\overline{u_i u_j}}{k}(P - \epsilon) \tag{8}$$

the Reynolds Eq. (7) becomes

$$\frac{\overline{u_i u_j}}{k}(P - \epsilon) = P_{ij} + 2\frac{\partial U_p}{\partial x_q}(I_{pjqi}^{(0)} + I_{piqj}^{(0)}) - \left(\phi_{ij}^{(0)} + \frac{2}{3}\delta_{ij}\right)\epsilon$$

$$+ \left[4C_1 k\left(\frac{\partial U_i}{\partial x_j} + \frac{\partial U_j}{\partial x_i}\right) + C_2 b_{ij}\epsilon\right]\frac{l}{y}F^\alpha + R_{ij} \tag{9}$$

where

$$P = -\overline{u_k u_l}\frac{\partial U_k}{\partial x_l}, \qquad P_{ij} = -\overline{u_i u_k}\frac{\partial U_j}{\partial x_k} - \overline{u_j u_k}\frac{\partial U_i}{\partial x_k}$$

$$R_{ij} = -\Omega_p(\epsilon_{ipk}\overline{u_j u_k} + \epsilon_{jpk}\overline{u_i u_k})$$

The realizability conditions and the wall modeling suggested by Shih and Lumley[16] are incorporated into this equation. Equation (9) is an algebraic equation for the Reynolds stresses. With tedious algebraic manipulation after neglecting higher-order terms, the individual components of the Reynolds stresses can be expressed as follows:

$$A_{11}\frac{\overline{u_1 u_1}}{k} = B_1 - \left(A_{12}\frac{\overline{u_2 u_2}}{k} + A_{13}\frac{\overline{u_3 u_3}}{k} + A_{14}\frac{\overline{u_1 u_2}}{k}\right.$$

$$+ A_{15}\frac{\overline{u_1 u_3}}{k} + A_{16}\frac{\overline{u_2 u_3}}{k}\right) \tag{10}$$

$$A_{22}\frac{\overline{u_2 u_2}}{k} = B_2 - \left(A_{21}\frac{\overline{u_1 u_1}}{k} + A_{23}\frac{\overline{u_3 u_3}}{k} + A_{24}\frac{\overline{u_1 u_2}}{k}\right.$$

$$+ A_{25}\frac{\overline{u_1 u_3}}{k} + A_{26}\frac{\overline{u_2 u_3}}{k}\right) \tag{11}$$

$$A_{33}\frac{\overline{u_3 u_3}}{k} = B_3 - \left(A_{31}\frac{\overline{u_1 u_1}}{k} + A_{32}\frac{\overline{u_2 u_2}}{k} + A_{34}\frac{\overline{u_1 u_2}}{k}\right.$$

$$+ A_{35}\frac{\overline{u_1 u_3}}{k} + A_{36}\frac{\overline{u_2 u_3}}{k}\right) \tag{12}$$

$$A_{44}\frac{\overline{u_1 u_2}}{k} = B_4 - \left(A_{41}\frac{\overline{u_1 u_1}}{k} + A_{42}\frac{\overline{u_2 u_2}}{k} + A_{43}\frac{\overline{u_3 u_3}}{k} \right.$$
$$\left. + A_{45}\frac{\overline{u_1 u_3}}{k} + A_{46}\frac{\overline{u_2 u_3}}{k} \right) \tag{13}$$

$$A_{55}\frac{\overline{u_1 u_3}}{k} = B_5 - \left(A_{51}\frac{\overline{u_1 u_1}}{k} + A_{52}\frac{\overline{u_2 u_2}}{k} + A_{53}\frac{\overline{u_3 u_3}}{k} \right.$$
$$\left. + A_{54}\frac{\overline{u_1 u_2}}{k} + A_{56}\frac{\overline{u_2 u_3}}{k} \right) \tag{14}$$

$$A_{66}\frac{\overline{u_2 u_3}}{k} = B_6 - \left(A_{61}\frac{\overline{u_1 u_1}}{k} + A_{62}\frac{\overline{u_2 u_2}}{k} + A_{63}\frac{\overline{u_3 u_3}}{k} \right.$$
$$\left. + A_{64}\frac{\overline{u_1 u_2}}{k} + A_{65}\frac{\overline{u_1 u_3}}{k} \right) \tag{15}$$

These equations are fully coupled to each other, and they can be rearranged and written as a matrix form

$$AX = B \tag{16}$$

where

$$A = \begin{bmatrix} A_{11} & A_{12} & A_{13} & A_{14} & A_{15} & A_{16} \\ A_{21} & A_{22} & A_{23} & A_{24} & A_{25} & A_{26} \\ A_{31} & A_{32} & A_{33} & A_{34} & A_{35} & A_{36} \\ A_{41} & A_{42} & A_{43} & A_{44} & A_{45} & A_{46} \\ A_{51} & A_{52} & A_{53} & A_{54} & A_{55} & A_{56} \\ A_{61} & A_{62} & A_{63} & A_{64} & A_{65} & A_{66} \end{bmatrix}$$

$$X = \frac{1}{k}\begin{bmatrix} \overline{u_1 u_1} \\ \overline{u_2 u_2} \\ \overline{u_3 u_3} \\ \overline{u_1 u_2} \\ \overline{u_1 u_3} \\ \overline{u_2 u_3} \end{bmatrix} \qquad B = \begin{bmatrix} B_1 \\ B_2 \\ B_3 \\ B_4 \\ B_5 \\ B_6 \end{bmatrix}$$

Expressions for the components of matrices A_{ij} and B_i are given in the Appendix.

k-ϵ Turbulence Model

To use the above ARSM model, the kinetic energy k, and the dissipation rate ϵ of turbulent motion have to be determined from the transport equations. The k-ϵ model was first developed by Jones and Launder[17] for two-dimensional flow and modified and extended by many researchers. In the case of the boundary-layer computation discussed herein, the k-ϵ transport equations must be consistent with the momentum equations. Therefore, the boundary-layer approximation is made in the derivation of the k-ϵ equation. The final reduced form of the k-ϵ equation in Levy-Lee coordinates is given by (see Ref. 18 for detailed derivation):

k Equation

$$\frac{\partial}{\partial \xi_3}\left[\frac{\bar{\mu}_k}{\bar{\mu}_{ref}}\frac{\partial k}{\partial \xi_3} \right] - V\frac{\partial k}{\partial \xi_3} - D_1 F\frac{\partial k}{\partial \xi_1} - D_2 G\frac{\partial k}{\partial \xi_2} + D_3 - D_6 \epsilon = 0 \tag{17}$$

ϵ Equation

$$\frac{\partial}{\partial \xi_3}\left[\frac{\bar{\mu}_\epsilon}{\bar{\mu}_{ref}}\frac{\partial \epsilon}{\partial \xi_3} \right] - V\frac{\partial \epsilon}{\partial \xi_3} - D_1 F\frac{\partial \epsilon}{\partial \xi_1} - D_2 G\frac{\partial \epsilon}{\partial \xi_2}$$
$$+ D_4\frac{\epsilon}{k} - D_5\frac{\epsilon^2}{k} = 0 \tag{18}$$

where

$$D_1 = 2\xi_1\frac{q_0}{q}, \qquad D_2 = \frac{U_{ref}}{U_{1e}}\frac{H_1}{H_2}\frac{2\xi_1}{q}$$

$$D_3 = P_k\frac{H_1}{U_{1e}}\frac{2\xi_1}{q}, \qquad D_4 = c_1 P_k\frac{H_1}{U_{1e}}\frac{2\xi_1}{q}$$

$$D_5 = c_2\frac{H_1}{U_{1e}}\frac{2\xi_1}{q}, \qquad D_6 = \frac{H_1}{U_{1e}}\frac{2\xi_1}{q}$$

$$\bar{\mu}_k = \frac{\mu_t}{\mu\sigma_k}, \quad \bar{\mu}_\epsilon = \frac{\mu_t}{\mu\sigma_\epsilon}, \quad c_1 = 1.44, \quad c_2 = 1.92$$

$$\sigma_k = 1.0, \quad \sigma_\epsilon = 1.3$$

The k-ϵ equations are valid in the region of high Reynolds numbers (based on local velocities). In the vicinity of the wall surface, viscous effects are dominant, and the local velocities are small; therefore, the presumed high Reynolds number (local) condition is no longer valid. A common way to handle the near-wall region is to use the wall-function technique in which the first grid point away from a wall is placed outside the viscous sublayer, and the kinetic energy and dissipation are prescribed at this point based on a law-of-the-wall formula. The k and ϵ can then be evaluated using the following formulas:

$$k_1 = \frac{U_\tau^2}{\sqrt{c_\mu}}, \qquad \epsilon_1 = \frac{U_\tau^3}{\kappa y_1} \tag{19}$$

where the subscript 1 refers to the first grid point outside the viscous sublayer and $\kappa = 0.4$ is von Kármán's constant. These values for k and ϵ are then used as the boundary conditions for the k-ϵ equations, which are solved for the rest of the flowfield. The boundary conditions for the k-ϵ equations at the boundary-layer edge are usually given by

$$\frac{\partial k}{\partial x_3} = 0, \qquad \frac{\partial \epsilon}{\partial x_3} = 0 \tag{20}$$

or by the specified values

$$k_e = \text{const}, \qquad \epsilon_e = \text{const}$$

It should be noted here that wall functions are used only for k and ϵ. The evaluations of the mean velocities (U,V,W) and the turbulent stresses $(\overline{u_i u_j})$ employ no wall functions.

Differencing Scheme and Solution Algorithm

The three-dimensional boundary-layer equations given by Eqs. (1–3) and the turbulent kinetic energy and dissipation equations given by Eqs. (17) and (18) are nonlinear partial differential equations. The boundary conditions and the inflow conditions used for the momentum equations are the same as those applied in Ref. 7.

The numerical differencing for the boundary-layer governing equations has been formulated in Refs. 7 and 9. To be consistent with the momentum equations, the k-ϵ equations are also approximated in a similar manner. The finite-difference operators used for both the boundary-layer equations and the turbulence equations are as follows:

$$\frac{\partial Q}{\partial \xi_1} = \frac{(Q_{I,J}^K - Q_{I-1,J}^K)}{\xi_{1,J} - \xi_{1,J-1}} \tag{21}$$

$$\frac{\partial Q}{\partial \xi_2} = \frac{Q_{I,J}^K - Q_{I,J-1}^K}{\xi_{2,J} - \xi_{2,J-1}} \qquad U_2 > 0$$

$$= \frac{Q_{I-1,J+1}^K - Q_{I-1,J}^K}{\xi_{2,J+1} - \xi_{2,J}} \qquad U_2 < 0 \tag{22}$$

$$\frac{\partial Q}{\partial \xi_3} = \frac{Q_{I,J}^{K+1} - Q_{I,J}^{K-1}}{\xi_3^{K+1} - \xi_3^{K-1}} \tag{23}$$

$$\frac{\partial}{\partial \xi_3}\left[\bar{\mu}\frac{\partial Q}{\partial \xi_3}\right] = \frac{\bar{\mu}^K + \bar{\mu}^{K+1}}{\xi_3^{K+1} + \xi_3^{K-1}} \frac{Q_{I,J}^{K+1} - Q_{I,J}^{K}}{\xi_3^{K+1} - \xi_3^{K}}$$

$$- \frac{\bar{\mu}^K + \bar{\mu}^{K-1}}{\xi_3^{K+1} - \xi_3^{K-1}} \frac{Q_{I,J}^{K} - Q_{I,J}^{K-1}}{\xi_3^{K} - \xi_3^{K-1}} \tag{24}$$

where Q represents a general function (F, G, V, H, k, or ϵ) and the subscripts I,J,K refer to the streamwise ξ_1, spanwise ξ_2, and normal ξ_3 locations, respectively. For crossflow derivatives, an upwind difference approximation is used depending upon the crossflow direction in order not to violate the criteria of the zone of dependence.

The resulting difference equations are reorganized to form a set of algebraic equations. The algebraic equations are nonlinear and are quasilinearized by solving them in an iterative manner. The linearized matrix equations for the mean flow are solved by the block substitution algorithm described in Refs. 7 and 9. The linearized matrix equations for turbulence are solved by a standard block tridiagonal solution algorithm.

The boundary-layer equations and the turbulence kinetic energy and dissipation equations are solved in an uncoupled manner. Both the boundary-layer and k-ϵ equations have two similar matrix forms and can be solved in a similar way. The k-ϵ equations are solved by lagging one step in the streamwise direction, i.e., the solution of the k-ϵ equations at the current step is achieved by using the velocity solution at the previous step. The ARSM [Eqs. (10–15)] is then solved by using the known values of k and ε.

Three-Dimensional, Turbulent, Pressure-Driven Boundary Layer

The boundary-layer computation method described in the previous section was used to compute the behavior of a three-dimensional, pressure-driven boundary layer and boundary layer on a turbomachinery rotor blade. The method was initially validated by computing the boundary layer developing on a flat plate. The prediction agrees very well with an analytical solution and well-documented experimental data for a flat-plate turbulent boundary.[18]

Muller[19] carried out comprehensive measurements of the mean flowfield and the Reynolds stress in a three-dimensional, pressure-driven boundary layer. The experimental setup is illustrated in Fig. 2. The flowfield external to the boundary layer was deflected laterally by turning vanes so
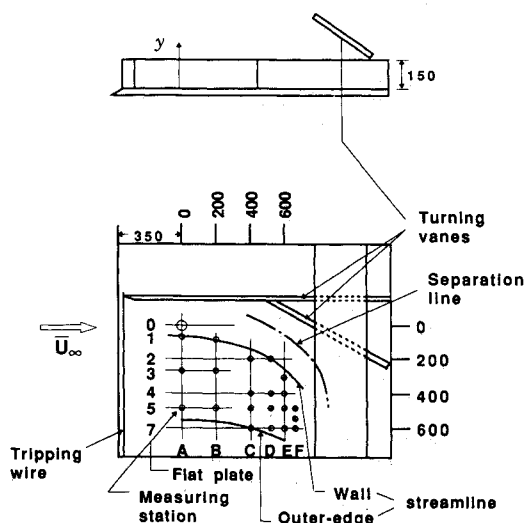
that streamwise flow deceleration occurred simultaneously with crossflow acceleration. The unit Reynolds number U_∞/v was 1.95×10^6 m^{-1}. The experimental accuracies quoted by Muller are as follows: $C_p = \pm 5 \times 10^{-3}$, $U_1 = \pm 1\%$, and $\overline{u_i u_j} = \pm 10\%$. As indicated in Fig. 2, the measuring stations are labeled with letters for the increasing x coordinate and with numbers for increasing the z coordinate. The measured pressure field is used as the input. There are $40 \times 40 \times 41$ grid points used in the computation.

The computed mean velocity profiles are shown in comparison with experimental data at several locations in Fig. 3. In the figure, L is the reference length, $L = 1$ m. The streamwise velocity U_1 is well predicted at all locations. The agreement between the prediction and the measurement of U_1 is excellent near the wall and in the outer layer and good to fair in the buffer region (the region between the outer and inner layers). Predictions are good even at D_5, where there is considerable flow turning and appreciable secondary flow (maximum of 10% of U_1). Considering the complexity of this flow, the secondary flow (U_2) prediction is excellent near the wall, very good at station B_5, and good to fair in outer layers at C_5 and D_5.

Also shown in Fig. 3 are predictions with the algebraic eddy viscosity model,[20] the k-ϵ model, and the ARSM/k-ϵ model. There is not much difference in the quality of the predictions; i.e., all models performed equally well. The complex strain effect in this case is small, and the boundary layer is mildly three dimensional. This may account for the good predictions with all of the turbulence models.

The turbulence intensities in the streamwise $(\overline{u_1 u_1})$, crossflow $(\overline{u_2 u_2})$, and normal directions $(\overline{u_3 u_3})$ predicted from the boundary-layer code and the ARSM model are shown in Fig. 4. It should be noted that none of the other models are capable of predicting these intensities, as the Reynolds stress transport equations are not utilized in k-ε and algebraic eddy viscosity models. The predictions of $\overline{u_1 u_1}$ and $\overline{u_2 u_2}$ profiles are excellent, including those in the wall regions. The prediction of $\overline{u_3 u_3}$ is excellent in the near-wall region but poor in the outer region. This is probably caused by inadequate prediction of the crossflow velocity profiles in this region (see Fig. 3). The excellent predictions for the intensities in the near-wall region are because the ARSM model satisfies the realizability condition and employs the wall function only for k and ϵ. There is no wall function used for the mean velocities or the Reynolds stresses.

The Reynolds shear-stress profiles in the streamwise $(\overline{u_1 u_2})$ and crossflow $(\overline{u_2 u_3})$ directions are shown in Fig. 5. The predictions for shear stresses are reasonably good considering the difficulty in measuring as well as predicting these quanti-
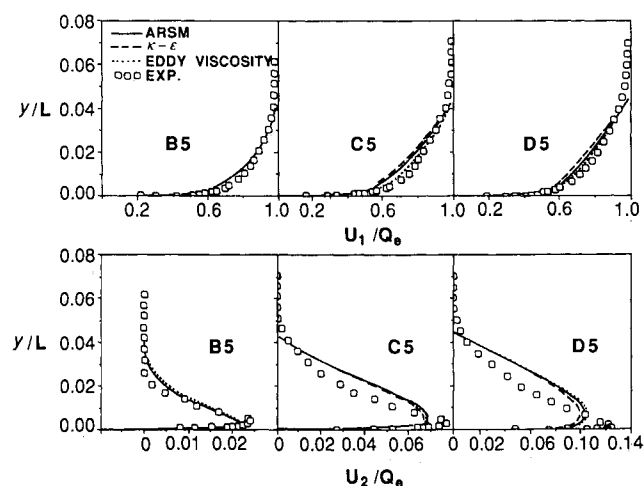

Fig. 2 Schematic of Muller's experimental setup (all dimensions are in mm).

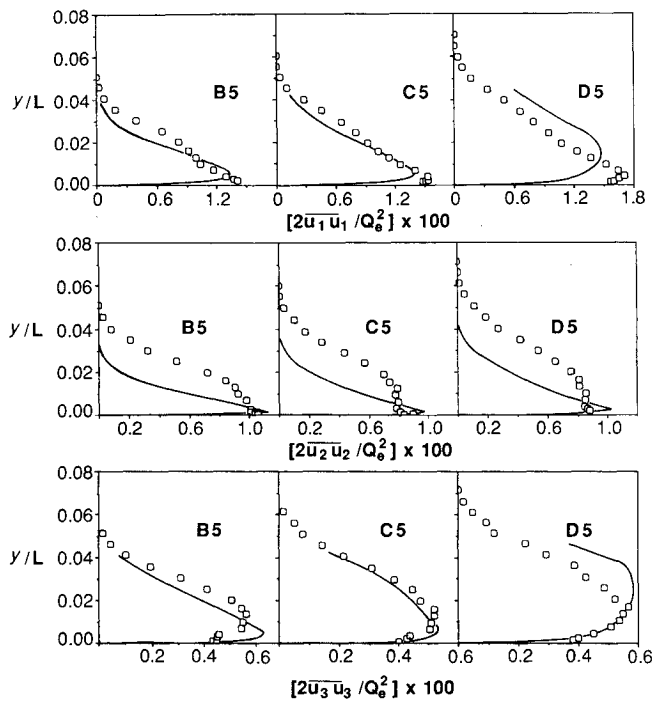Fig. 3 Mean velocity U_1 and U_2 profiles of three-dimensional boundary layer (Muller).

Fig. 4 Reynolds stress $\overline{u_i u_i}$ profiles of three-dimensional boundary layer (Muller); for legend see Figs. 2 and 3.
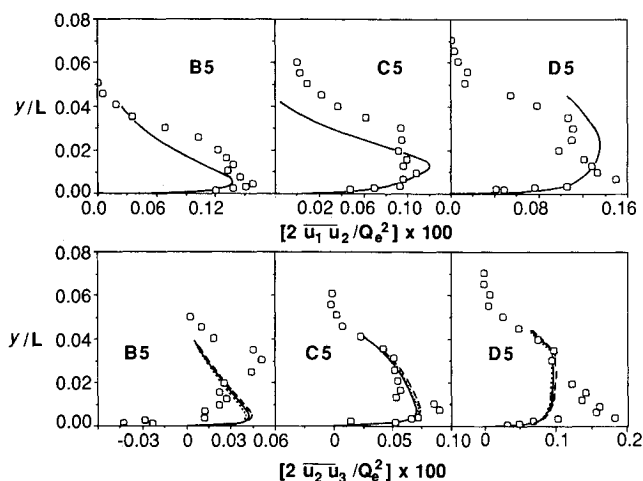

Fig. 5 Reynolds stress $\overline{u_i u_j}$ profiles of three-dimensional boundary layer (Muller); for legend see Figs. 2 and 3.

ties. Once again, the predictions in the near-wall region are excellent. The stresses in the crossflow direction, predicted from all three turbulence models, show very little difference. As mentioned earlier, these results are not surprising because the complex strain effect is small, and both the k-ϵ and the algebraic Reynolds stress models should work well.

Three-Dimensional, Turbulent, Boundary Layer on Compressor Rotor Blade

The three-dimensional boundary layer on the turbomachinery rotor blade is very different from the three-dimensional boundary layer on a flat plate. Pressure gradients exist in both the streamwise and the crossflow directions. The pressure field, which depends on the core flow, can cause a considerable change in the boundary-layer behavior. The geometry is another factor that greatly affects the boundary-layer behavior. The curvature of surfaces can stabilize or destabilize the boundary-layer flow. Perhaps the most important effect is the rotation, which introduces not only three dimensionality in
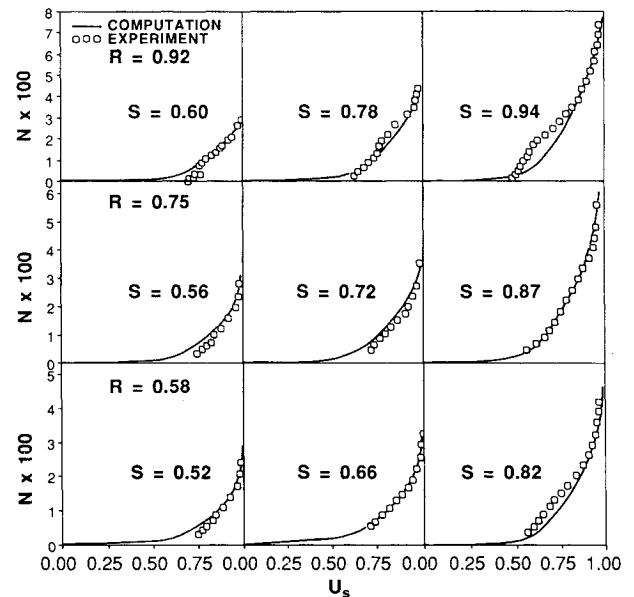

Fig. 6 Streamwise velocity profiles on suction surface of compressor rotor blade at $R = 0.58$, $R = 0.75$, and $R = 0.92$.

the mean flow, but also changes the structure of the turbulence as indicated in Ref. 10. All of these factors make the computation of three-dimensional boundary-layer development on rotor blades very challenging. The algorithm and the turbulence model should be capable of capturing the above effects.

Efforts were made to compute the three-dimensional, turbulent boundary layer on the rotor blade of an axial flow compressor facility. The details of the blade and the compressor are given in Ref. 21. This is a low-speed compressor with a hub-to-tip ratio of 0.5 and a 21-bladed rotor operating at the peak pressure rise coefficient. The chord length at the tip was 15.41 cm corresponding to a blade chord Reynolds number of 2.8×10^5. The blade spacing at the tip was 14.12 cm, the annulus wall diameter was 0.936 m, and the rotor speed was 1080 rpm. Extensive data have been acquired from this compressor rotor. Of these, the blade boundary-layer data are the most comprehensive and are used for comparison with the prediction. The experimental data were taken with a miniature two-sensor, hot wire rotating with the blade. The boundary-layer data show that no separation occurred in the flow. The measured pressure field is used as the input pressure data. There are 40 grid points along the streamwise direction, which cover from leading edge to trailing edge, 40 grid points along the spanwise direction, and 41 grid points in the normal direction perpendicular to the blade surface.

The boundary-layer predictions are carried out for the case of a flow coefficient ϕ of 0.5. Comprehensive predictions are presented here with the comparison of available experimental data from Ref. 22. Flow visualization indicated that transition occurred very close to the leading edge due to high freestream turbulence, and hence the flow was assumed to be turbulent right after the leading edge.

The predicted streamwise velocity profile on the suction surface of the blade is shown compared with the data in Fig. 6. The prediction shows excellent agreement with the experimental data. Not only is the outer layer of the blade boundary layer predicted well, but the inner layer prediction in most locations also agrees with the experimental data. The boundary-layer predictions are good at all spanwise locations (11, 50, and 84% of span from the tip). A slight overprediction in the inner layer exists near the midchord ($S \leq 0.6$) where the boundary layer is thin, but it disappears when the boundary layer thickens. These predictions are better than those from either a multipass space marching technique (Fig.

14 of Ref. 23) or a time marching technique (Figs. 9 and 10 of Ref. 24) in spite of the fact that both of these techniques solve the Navier-Stokes equations. This is because in view of the iterative nature of these techniques and the computer storage and CPU time required by them, only a few (7–10) grid points were used inside the boundary layer along the slip boundary conditions. The agreement between the measured and the predicted streamwise velocity field is fair for the full Navier-Stokes codes but excellent for the boundary-layer code. The radial velocity profiles predicted from the Navier-Stokes codes showed very poor agreement due to the coarse grid resolution and the slip boundary conditions. It might be possible to use a very fine grid and a "no-slip" boundary condition to improve the Navier-Stokes predictions, but the cost would be exorbitant. Moreover, due to artificial dissipation in these Navier-Stokes codes, numerical stability problems are encountered in integrating these equations down to the surface. This clearly reveals the advantage of the boundary-layer code for the viscous-layer prediction.

Good predictions are also obtained for the boundary layers on the pressure surface except in the regions of midchord, where boundary layers are extremely thin. These predictions are given in Ref. 18.

Radial velocity predictions on the suction surface are shown in Fig. 7. The quality of these predictions is quite good. Considering that the radial velocity is one order of magnitude smaller than the streamwise velocity, the radial velocities are difficult to predict. The predictions in most locations show excellent agreement with the measured data. The steep radial velocity gradient and maximum radial velocity near the wall are also predicted reasonably well. The predictions deviate at $R = 0.92$, where the tip clearance effects may be present. The prediction of radial velocities from space marching (Fig. 14 of Ref. 23) and time marching (Figs. 9 and 10 of Ref. 24) codes were poor due to an inadequate resolution of the wall region.

The computation was also carried out with the k-ϵ model and the algebraic eddy viscosity model. A comparison between the various models for $R = 0.95$, $S = 0.72$ and $S = 0.87$ is shown in Fig. 8. For the streamwise velocity, the predictions with the ARSM model is the most accurate; although the predictions with k-ϵ and algebraic eddy viscosity models are fair. For the radial velocity, the ARSM model has obvious advantages over the k-ϵ model and the algebraic eddy viscosity model. The predictions with both the k-ϵ model and

the algebraic eddy viscosity model underpredict the radial velocity. This improvement in velocity predictions with the ARSM model is as expected. Curvature and rotation effects make the high-order turbulence model necessary in the prediction of turbomachinery rotor flow. The lower-order models, such as algebraic eddy viscosity and k-ϵ models, do not have the capability of capturing these effects.

The predictions of the streamwise momentum thickness for the suction side are compared with the experimental data in Fig. 9. The momentum thickness is defined as

$$\theta_{11} = \int_0^\delta \frac{U_s}{U_e}\left(-\frac{U_s}{U_e}\right)dn \qquad (25)$$

where δ is the boundary-layer thickness (normalized by local chord length). The momentum thickness is an integral quantity that depends on the boundary-layer profile and thickness. Any error in the boundary-layer prediction will compound the difficulty in predicting the momentum thickness. Here again, the predictions are excellent, even near the tip and the hub walls, indicating the ability of this code to predict profile losses and efficiency.

The above computations were carried out using a VAX 8550 computer. Convergence of the solution is good. The
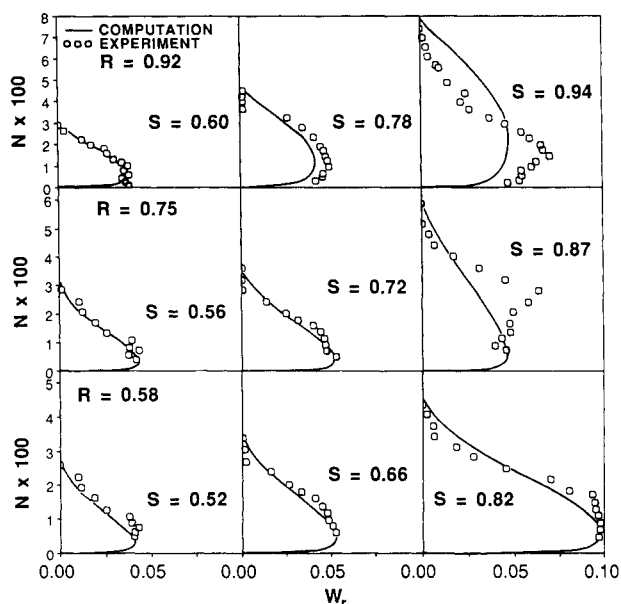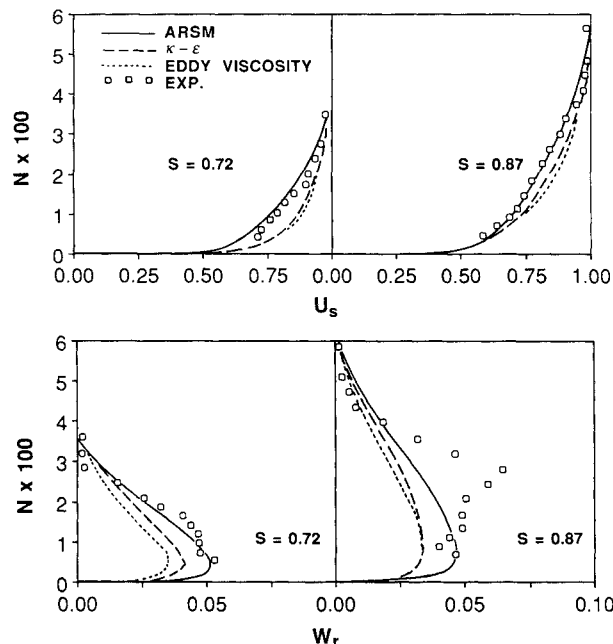

Fig. 8   Mean velocity profiles on suction surface of compressor rotor blade at $R = 0.75$—comparison of turbulence models.
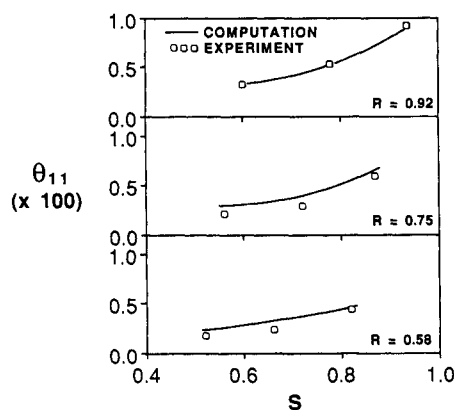

Fig. 9   Streamwise momentum thickness distribution for suction surface of compressor rotor blade.

Fig. 7   Radial velocity profiles on suction surface of compressor rotor blade at $R = 0.58$, $R = 0.75$, and $R = 0.92$.

convergence criteria used in the computation is

$$|f_{i,j,k}^{n+1} - f_{i,j,k}^{n}| < a$$

where f is any solution parameter $(F,G,k,\epsilon,$ etc.), i,j,k are space location indices, n is the iteration index, and a was taken as 0.0001 in the computation. It usually takes 3–5 iterations to converge a solution at every grid point. The computation is also very efficient. For a grid $40 \times 40 \times 41$, it takes 4 min of CPU time on the VAX 8550 to get a fully converged solution for a compressor rotor-blade boundary layer.

Concluding Remarks

A three-dimensional, turbulent boundary-layer solution method is applied to predict the behavior of the boundary layers on a rotor blade of an axial flow compressor, and a pressure-driven, three-dimensional boundary-layer flow. A new ARSM is developed and used in the computational algorithm in combination with turbulent kinetic energy and dissipation $(k$-$\epsilon)$ equations. The boundary-layer and k-ϵ equations are solved in the same manner but in an uncoupled form. The prediction of the three-dimensional, turbulent boundary layers on a rotor blade and a pressure-driven, turbulent boundary layer are good.

A higher-order turbulence model is necessary for predicting three-dimensional, boundary-layer development on rotor blades since simple models cannot resolve the complex strain field. In three-dimensional, boundary-layer computations, the new ARSM/k-ϵ model is most accurate compared to the algebraic eddy viscosity model and the k-ϵ model, especially for shear layers subjected to rotation and curvature. Furthermore, the boundary-layer codes in a marching mode are computationally very efficient and could be integrated with the Navier-Stokes codes to resolve the viscous layers accurately through the use of dense grids and higher-order turbulence models.

Appendix

Expressions for the matrix components A_{ij} and B_i in Eq. (16) are given below.

$$A_{11} = P - \epsilon\left(1 + \frac{C_2}{2}\frac{l}{y}F^\alpha - \frac{\beta}{2}\right)$$

$$A_{14} = -\frac{k}{3}\frac{\partial U_1}{\partial x_2}(2 - C_{1f} + C_{2f}) - 4\Omega_3 k$$

$$A_{15} = -\frac{k}{15}\frac{\partial U_1}{\partial x_3}(10 - 2C_{1f} + 5C_{2f}) + 4\Omega_2 k$$

$$A_{16} = -2k\frac{\partial U_2}{\partial x_3}(C_{1f} + C_{2f})$$

$$A_{22} = P - \epsilon\left(1 + \frac{C_2}{2}\frac{l}{y}F^\alpha - \frac{\beta}{2}\right)$$

$$A_{24} = -\frac{k}{6}\frac{\partial U_1}{\partial x_2}(-4 + C_{1f} + 2C_{2f}) - 4\Omega_3 k$$

$$A_{25} = -\frac{k}{5}\frac{\partial U_1}{\partial x_3}(-C_{1f} + C_{2f})$$

$$A_{26} = -\frac{2k}{15}\frac{\partial U_2}{\partial x_3}(5 - C_{1f}) + 4\Omega_1 k$$

$$A_{33} = P - \epsilon\left(1 + \frac{C_2}{2}\frac{l}{y}F^\alpha - \frac{\beta}{2}\right)$$

$$A_{34} = -\frac{k}{5}\frac{\partial U_1}{\partial x_2}(-C_{1f} + C_{2f})$$

$$A_{35} = -\frac{k}{3}\frac{\partial U_1}{\partial x_3}(-2 + C_{1f} + C_{2f}) - 4\Omega_2 k$$

$$A_{36} = -\frac{k}{3}\frac{\partial U_2}{\partial x_3}(-2 + C_{1f} + C_{2f}) + 4\Omega_1 k$$

$$A_{41} = -\frac{k}{15}\frac{\partial U_1}{\partial x_2}(4C_{1f} + C_{2f} - 5) + 2\Omega_3 k$$

$$A_{42} = -\frac{k}{30}\frac{\partial U_1}{\partial x_2}(C_{1f} - 2C_{2f} - 10) - 2\Omega_3 k$$

$$A_{44} = P - \epsilon\left(1 - \frac{\beta}{2} + \frac{C_2}{2}\frac{l}{y}F^\alpha\right)$$

$$A_{45} = -\frac{k}{30}\frac{\partial U_2}{\partial x_3}(10 + C_{1f} - 2C_{2f}) - 2\Omega_1 k$$

$$A_{46} = -\frac{k}{30}\frac{\partial U_1}{\partial x_3}(10 + C_{1f} - 2C_{2f}) + 2\Omega_2 k$$

$$A_{51} = -\frac{k}{15}\frac{\partial U_1}{\partial x_3}(4C_{1f} + C_{2f} - 5) - 2\Omega_2 k$$

$$A_{53} = -\frac{k}{30}\frac{\partial U_1}{\partial x_3}(C_{1f} - 2C_{2f} - 10) + 2\Omega_2 k$$

$$A_{54} = -\frac{k}{15}\frac{\partial U_2}{\partial x_3}(4C_{1f} + C_{2f} - 5) + 2\Omega_1 k$$

$$A_{55} = P - \epsilon\left(1 - \frac{\beta}{2} + \frac{C_2}{2}\frac{l}{y}F^\alpha\right)$$

$$A_{56} = -\frac{k}{30}\frac{\partial U_1}{\partial x_2}(10 + C_{1f} - 2C_{2f}) - 2\Omega_3 k$$

$$A_{62} = -\frac{k}{15}\frac{\partial U_2}{\partial x_3}(4C_{1f} + C_{2f} - 5) + 2\Omega_1 k$$

$$A_{63} = -\frac{k}{30}\frac{\partial U_2}{\partial x_3}(C_{1f} - 2C_{2f} + 10) - 2\Omega_1 k$$

$$A_{64} = -\frac{k}{15}\frac{\partial U_1}{\partial x_3}(4C_{1f} + C_{2f} - 5) - 2\Omega_2 k$$

$$A_{65} = -\frac{k}{15}\frac{\partial U_1}{\partial x_2}(4C_{1f} + C_{2f} - 5) + 2\Omega_3 k$$

$$A_{66} = P - \epsilon\left(1 - \frac{\beta}{2} + \frac{C_2}{2}\frac{l}{y}F^\alpha\right)$$

$$A_{12} = A_{13} = A_{21} = A_{23} = A_{31} = A_{32} = A_{43} = A_{52} = A_{61} = 0$$

$$B_1 = -P_{11} - \left(\frac{2}{3} - \frac{1}{3}\beta\right)\epsilon + \left(8C_1 k\frac{\partial U_1}{\partial x_1} - \frac{C_2}{3}\epsilon\right)\frac{l}{y}F^\alpha$$

$$B_2 = -P_{22} - \left(\frac{2}{3} - \frac{1}{3}\beta\right)\epsilon + \left(8C_1 k\frac{\partial U_2}{\partial x_2} - \frac{C_2}{3}\epsilon\right)\frac{l}{y}F^\alpha$$

$$B_3 = -P_{33} - \left(\frac{2}{3} - \frac{1}{3}\beta\right)\epsilon + \left(8C_1 k\frac{\partial U_3}{\partial x_3} - \frac{C_2}{3}\epsilon\right)\frac{l}{y}F^\alpha$$

$$B_4 = -P_{12} + \frac{k}{5}\frac{\partial U_1}{\partial x_2}(1 - C_{1f}) + 4C_1 k\left(\frac{\partial U_1}{\partial x_2} + \frac{\partial U_2}{\partial x_1}\right)\frac{l}{y}F^\alpha$$

$$B_5 = -P_{13} + \frac{k}{15}\frac{\partial U_1}{\partial x_3}(3 - 5C_{1f}) + 4C_1 k\left(\frac{\partial U_1}{\partial x_3} + \frac{\partial U_3}{\partial x_1}\right)\frac{l}{y}F^\alpha$$

$$B_6 = -P_{23} - \frac{k}{5}\frac{\partial U_2}{\partial x_3}(1 - C_{1f}) + 4C_1 k\left(\frac{\partial U_2}{\partial x_3} + \frac{\partial U_3}{\partial x_2}\right)\frac{l}{y}F^\alpha$$

extensively in this program. Part of the turbulence modeling effort was carried out by B. Lakshminarayana during his sabbatical at The Institute for Fluid Mechanics, Ecole Centrale de Lyon, where he was a visiting professor supported partially by Centre National De La Recherche Scientifique, Ministere de L'Educational Nationale and the U.S. National Science Foundation (Grant INT-87-02083, U.S.-Industrialized Countries Program for the exchange of Scientists and Engineers).

References

[1]Lakshminarayana, B., and Govindan, T. R., "Analysis of Turbulent Boundary Layer on Cascade and Rotor Blades of Turbomachinery," *AIAA Journal*, Vol. 19, Oct. 1981, pp. 1333–1341.

[2]Thompkins, W. T., and Usab, W. J., Jr., "A Quasi-Three Dimensional Blade Surface Boundary Layer Analysis for Rotating Blades," *ASME Journal of Engineering for Power*, Vol. 104, April 1982, p. 439.

[3]Nash, J. F., and Patel, V. C., "Three Dimensional Turbulent Boundary Layers," Scientific and Buisiness Consultants, Inc., Atlanta, GA, 1972.

[4]Cebeci, T., Kaups, K., and Ramsey, J. A., "A General Method for Calculating Three Dimensional Compressible Laminar and Turbulent Boundary Layers," NASA CR-2777, 1977.

[5]Lakshminarayana, B., "Three Dimensional Turbulent Boundary Layers," Von Karman Institute Lecture Series, Belgium LS 83-03, 1982.

[6]Cousteix, J., "Computation of Three Dimensional Boundary Layer Including Separation," AGARD NATO Rept. R. 741, 1986.

[7]Vatsa, V.N., "A Three-Dimensional Boundary Layer Analysis Including Heat Transfer and Blade Rotation Effects," Third Symposium on Numerical and Physical Aspects of Aerodynamic Flows, Long Beach, CA, 1985.

[8]Anderson, O. L., "Assessment of a 3-D Boundary Layer Analysis to Predict Heat Transfer and Flow Field in a Turbine Passage," NASA CR-174894, 1985.

[9]Anderson, O. L., "Calculation of Three-Dimensional Boundary Layers on Rotating Turbine Blades," *Journal of Fluid Engineering*, Vol. 109, March 1987, pp. 41–50.

[10]Lakshminarayana, B., "Turbulence Modeling for Complex Flows," *AIAA Journal*, Vol. 24, Dec. 1986, p. 1900.

[11]Dhawan, S., and Narasimha, R., "Some Properties of Boundary Layer Flow During Transition from Laminar to Turbulent Motion," *Journal of Fluid Mechanics*, Vol. 3, 1958, pp. 418–436.

[12]Rodi, W., "A New Algebraic Relation for Calculating Reynolds Stresses," *ZAMM*, Vol. 56, 1976, p. 219.

[13]Galmes, J. M., and Lakshminarayana, B., "Turbulence Modeling for Three Dimensional Shear Flows over Curved Rotating Bodies," *AIAA Journal*, Vol. 22, Oct. 1984, pp. 1420–1428.

[14]Rodi, W., and Scheuerer, G., "Calculations of Curved Shear Layers in Two Equation Turbulence Models," *Physics of Fluids*, Vol. 26, 1983, pp. 1422–1436.

[15]Warfield, M., and Lakshminarayana, B., "Computation of Rotating Turbulent Flow with an Algebraic Reynolds Stress Model," *AIAA Journal*, Vol. 25, July 1987, pp. 957–964.

[16]Shih, T-H., and Lumley, J. L., "Second-Order Modeling of Near-Wall Turbulence," *Physics of Fluids*, Vol. 29, 1986, pp. 971–975.

[17]Jones, W. P., and Launder, B. E., "The Prediction of Laminarization with a Two-Equation Model of Turbulence," *International Journal of Heat and Mass Transfer*, Vol. 15, 1972, pp. 301–314.

[18]Zhang, J., "An Experimental, Analytical, and Computational Investigation of Turbomachinery Rotor Flow Field," Ph.D. Thesis, Department of Aerospace Engineering, The Pennsylvania State Univ., University Park, PA, 1988.

[19]Muller, U. R., "Measurement of the Reynolds Stresses and the Mean-Flow Field in a Three Dimensional Pressure Driven Boundary Layer," *Journal of Fluid Mechanics*, Vol. 119, 1982, pp. 121–150.

[20]Baldwin, B. S., and Lomax, H., "Thin Layer Approximation and Algebraic Model for Separation Flows," AIAA Paper 78-257, 1978.

[21]Sitaram, N., and Lakshminarayana, B., "End Wall Flow Characteristics and Overall Performance of a Compressor Rotor," NASA CR-3671, 1983.

[22]Lakshminarayana, B., and Popovski, P., "Three-Dimensional Boundary Layer on a Compressor Rotor Blade at Peak Pressure Rise Coefficient," *ASME Journal of Turbomachinery*, Vol. 109, No. 1, Jan. 1987, pp. 91–98.

[23]Kirtley, K. R., and Lakshminarayana, B., "Computation of 3-D Turbulent Turbomachinery Flows Using a Coupled Parabolic-Marching Method," American Society of Mechanical Engineers, New York, Paper 88-GT-80, 1988.

[24]Warfield, J. M., and Lakshminarayana, B., "Calculation of a Three Dimensional Turbomachinery Rotor Flow with a Navier-Stokes Code," American Society of Mechanical Engineers, New York, Paper 87-GT-232, 1987.